



Iranian wetland inventory map at a spatial resolution of 10 m using Sentinel-1 and Sentinel-2 data on the Google Earth Engine cloud computing platform

MohammadAli Hemati ·
Mahdi Hasanlou · Masoud Mahdianpari ·
Fariba Mohammadimanesh

Received: 5 January 2022 / Accepted: 1 April 2023 / Published online: 13 April 2023
© The Author(s), under exclusive licence to Springer Nature Switzerland AG 2023

Abstract Detailed wetland inventories and information about the spatial arrangement and the extent of wetland types across the Earth's surface are crucially important for resource assessment and sustainable management. In addition, it is crucial to update these inventories due to the highly dynamic characteristics of the wetlands. Remote sensing technologies capturing high-resolution and multi-temporal views of landscapes are incredibly beneficial in wetland mapping compared to traditional methods. Taking advantage of the Google Earth Engine's computational power and multi-source earth observation data from Sentinel-1 multi-spectral sensor and Sentinel-2 radar, we generated a 10 m nationwide wetlands inventory map for Iran. The whole country is mapped using an object-based image processing framework, containing SNIC

superpixel segmentation and a Random Forest classifier that was performed for four different ecological zones of Iran separately. Reference data was provided by different sources and through both field and office-based methods. Almost 70% of this data was used for the training stage and the other 30% for evaluation. The whole map overall accuracy was 96.39% and the producer's accuracy for wetland classes ranged from nearly 65 to 99%. It is estimated that 22,384 km² of Iran are covered with water bodies and wetland classes, and emergent and shrub-dominated are the most common wetland classes in Iran. Considering the water crisis that has been started in Iran, the resulting ever-demanding map of Iranian wetland sites offers remarkable information about wetland boundaries and spatial distribution of wetland species, and therefore it is helpful for both governmental and commercial sectors.

M. Hemati · M. Mahdianpari
Department of Electrical and Computer Engineering,
Memorial University of Newfoundland, St. John's, Canada
e-mail: mhemati@mun.ca

M. Mahdianpari
e-mail: m.mahdianpari@mun.ca

M. Hemati · M. Hasanlou (✉)
School of Surveying and Geospatial Engineering, College
of Engineering, University of Tehran, Tehran, Iran
e-mail: hasanlou@ut.ac.ir

M. Mahdianpari · F. Mohammadimanesh
C-CORE, 1 Morrissey Road, St. John's, Newfoundland/
Labrador A1B 3X5, Canada
e-mail: f.mohammadimanesh@c-core.ca

Keywords Wetland mapping · Google Earth Engine · Sentinel-2 · Sentinel-1 · Iran · Object-based Random Forest

Introduction

Wetlands are described as transitional terrains between aquatic systems and terrestrials. Water is the most contributing element in wetland areas, managing the environment and related animals' life and plants. In wetland environments, shallow water covers

the land, or the water level is near or at the surface. Under the text of the Ramsar Convention, the first intergovernmental treaty on the sustainable use and conservation of wetlands, wetlands are defined as: “areas of marsh, fen, peatland or water, whether natural or artificial, permanent or temporary, with water that is static or flowing, fresh, brackish or salt, including areas of marine water the depth of which at low tide does not exceed six meters” (Ramsar Convention Secretariat, 2013).

Wetlands’ designation to international or governmental conventions reflects the global importance of wetlands. It is estimated that wetland sites cover nearly 3 to 8% of the global land surface (Tiner et al., 2015). However, this small proportion has a significant impact on climate, biodiversity, and both natural and artificial ecosystems. A variety of environmental functions are offered by wetlands. They regulate hydrological cycles and mitigate floods and storms to protect shorelines. Wetlands supply fresh and clean water by retaining and stabilizing sediments, and they store a considerable amount of carbon and other nutrients (Mitsch et al., 2013).

Considering the importance of wetland ecosystems, they are being destroyed at an increasing rate because of both anthropogenic activities and natural cycles (Wulder et al., 2018). The Millennium Ecosystem Assessment found that wetlands are being lost faster than any other ecosystem on a global scale. Primary indirect drivers of the wetland changes are the population growth, and economic activities and overexploitation of wetland resources, water use, eutrophication and pollution, infrastructure development, overharvesting, and land conversion are the primary direct drivers of wetland loss and degradation (“Millennium Ecosystem Assessment” 2005).

Recognition of wetlands’ values as an important ecosystem and as a natural resource, growing interest in wetland mapping, and environmental change monitoring for governments and international organizations (Wulder et al., 2018). Wetland studies with traditional approaches that were based on a field survey of wetland ecosystems were time- and cost-consuming. Photogrammetry (Cox, 1992) and satellite imaging (Rundquist et al., 2001) gradually replaced these traditional approaches, and use of earth observation approaches in different applications, such as water level monitoring (Wdowinski et al., 2008), classification (Chopra et al., 2001), and change detection (Munyati, 2000), has been well illustrated.

Satellite remote sensing has many advantages for inventorying and monitoring wetlands, such as wide coverage, low cost, multi-temporal data, and information about land use in upland areas. Especially in developing countries, like Iran, where small information on wetland areas, surrounding uplands, and wetland losses are available and funds are limited, remote sensing technologies can be appropriate for wetland inventories and monitoring (Ozesmi & Bauer, 2002). However, wetland mapping over a large area has been a challenge or an impossible task to do until very recently, given the fact that wetlands have a highly dynamic nature and the high expense of in situ data collection for country-wide wetland mapping. New technologies and resources overcome this problem by providing free high-quality earth observation data on cloud computing platforms. An extensive archive of remote sensing data is accessible from the European Space Agency (ESA), National Aeronautics and Space Administration (NASA), United States Geological Survey (USGS), and National Oceanic and Atmospheric Administration (NOAA), and recent advancement of novel cloud-based computational platforms, like the Google Earth Engine (GEE), provide opportunities to apply state-of-the-art algorithms and machine learning advances for large-scale wetland mapping.

Considering the availability of cloud-free images, optical satellite imaging is practical for wetland classification (Adam et al., 2010; Hemati et al., 2021a, b). Although in northern latitude, tropical, and subtropical regions, optical satellite imagery is less useful due to high cloud cover almost all the year. On the contrary, images from Synthetic Aperture Radar (SAR) platforms are preferable when optical image usage is limited by cloud covers (Whiteside & Bartolo, 2015). These images are independent of weather or atmospheric conditions, can be acquired days and nights, and also can penetrate through the soil, vegetation, and tree canopies; therefore, a lot of attention has been gained by SAR images for wetland mapping (Schmitt & Brisco, 2013). Usage of single-polarization (Gessner et al., 2015), dual-polarization (Dabboor et al., 2015), and full-polarization (Gallant et al., 2014), in addition to polarimetric features, have been demonstrated in different applications regarding wetlands. For places with low coverage of clouds, like Iran, another consideration for wetland mapping would be the usage of multi-platform satellite images, especially the fusion of radar data and optical images (M. A.). The combination of optical and SAR images has been

comprehensively examined through different studies with different applications (Corcoran et al., 2013; Durieux et al., 2007; Li & Chen, 2005; Walker et al., 2010), showing promising results achieved by a combination of SAR and spectral data. The accessibility of optical and SAR images with high spatial resolution has been joined with cutting-edge image processing frameworks, like Object-Based Image Analysis (OBIA), to enhance the quality of final maps (Blaschke, 2010). The OBIA framework has been shown to have better results compared to pixel-based approaches, by combining multi-source earth observation data with various ground resolutions. Classification features, including textual, contextual, spatial, spectral, and geometric information, in addition to the real pixel values of an object (a group of neighborhood pixels), are provided by OBIA, enhancing the classification results (Salehi et al., 2012). Several studies have tested the potential of OBIA for the classification of wetland areas (Grenier et al., 2008; Walker et al., 2010). The segmentation step is typically followed by a classification to generate the final results. As a flexible ensemble learning method, Random Forest (RF) has acquired a great deal of attention in mapping the land cover and land use using remote sensing data recently (Ghimire et al., 2010; Guo et al., 2011; Rodriguez-Galiano et al., 2012). RF is an advanced and robust algorithm due to minimum affection of noises and outliers, great capability to process huge multi-source and high-dimensional datasets, and it usually achieves more accurate results compared to other advanced methods, such as support vector machine (Sheykhoumoua et al., 2020).

Leveraging cloud computing platforms, free high-resolution multi-temporal satellite images, and machine learning (ML), and deep learning (DL) methods, various studies have been implicated for mapping heterogeneity of wetland landscapes with a fusion of both SAR and spectral data (Amani et al., 2017; Mahdianpari et al., 2017; Rezaee et al., 2018; Salehi et al., 2019). National wetland mapping has been recently implicated in some countries (Mahdianpari et al., 2020a, b). Also, remote sensing technologies have been used for some major wetland sites in Iran (Alibakhshi et al., 2017; Qaderi Nasab & Rahnama, 2020; Qureshi et al., 2020). However, generally, these studies are only limited to a single wetland site and lack land cover maps with robust classification systems, including wetland subclasses and vegetation.

The overarching objective of this study with consideration of the above discussion was to fulfill the absence

of a wetland inventory map of Iran with an internationally accepted classification scheme and standard wetland terminology, including various wetland types founded in different climates of Iran, and by taking advantage of the special processing strength of cloud-computing platforms, and accessibility free earth observation data with high spatial resolution. Specifically, the synergistic usage of 10-m free optical and radar data from Sentinel missions, including Sentinel-2 multispectral images with a 10-day revisit time and Sentinel-1 SAR images with a 12-day revisit time, has been considered in this study. Also, we aimed to take advantage of OBIA and RF to process a huge amount of multi-source and high-dimensional data to achieve promising land cover results across the country.

Study area and classification system

Iran (the Islamic Republic of) is a country located in the southwest of Asia, between 25–40°N and 44–66°E, in the Middle East region (Fig. 1). With an area of 1.64 million km² and nearly 84 million population, Iran is the 17th largest and populated country in the world. Since 1955, the population of Iran has increased by 77%, and the urban population percentage has increased from 30 to 75% (UN, 2019). Population growth and human activities directly have a major impact on climate and land cover changes (Song et al., 2018). Due to high topographic and climatic diversity and its location at biogeographic realms crossroad, Iran is one of the most biodiverse countries, and around 1260 vertebrates with more than 8000 plants species have been identified there (Yousefi et al., 2019).

According to the Iranian Department of Environment, 138 wetland sites are registered locally in Iran (Fig. 1). The convention on globally important wetlands especially as waterfowl habitat (Ramsar Convention) was first founded in February 1971 on the southern shore of the Caspian Sea, in the Iranian city of Ramsar. Twenty-five wetland sites have been registered in the Ramsar convention from Iran with a total area of 14,886.24 km² (Table 1). Among the 42 Ramsar wetland types identified in the world, 30 wetland types from inland, marine, and human-made wetlands are found in Iran (Ramsar Convention Secretariat, 2013). Intermittent or seasonal freshwater marshes or inorganic soil pools, including seasonally flooded sedge marshes, meadows, sloughs, and potholes, are the most common wetland type found in Iran.

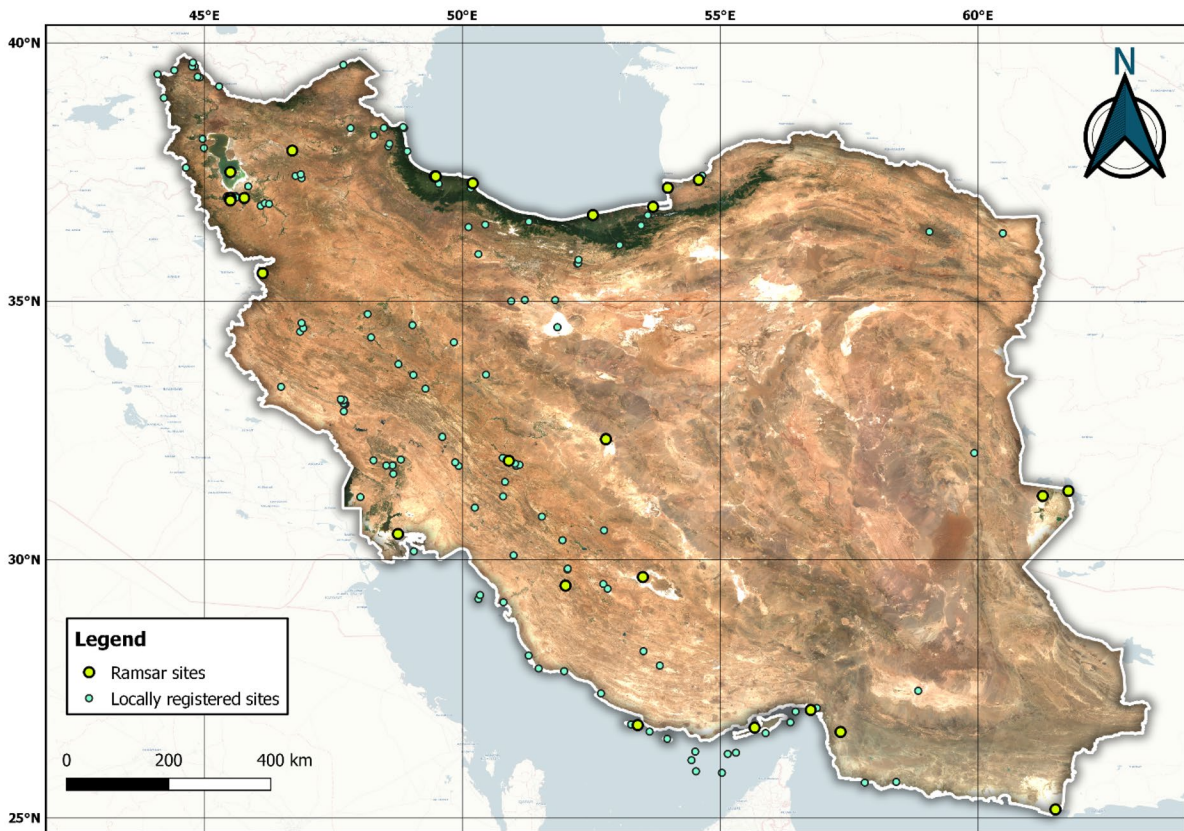


Fig. 1 Median Sentinel-2 image of the study area and location of wetland site centroids

Out of Iranian registered wetland sites, 21 are included in Ramsar Criterion 1, which means within the appropriate biogeographic region, they contain rare, unique, or representative wetland types and are considered internationally important. Unfortunately, the ecological characteristics of six Iranian Ramsar sites have changed, are changing, or are beginning to change because of pollution, technological advancements, or other human interference. These wetlands have been included in the Montreux Record to attract positive local and global conservation attention.

Many countries have regional and national wetland terminology, and they have adopted narrower definitions. National wetland classification systems are designed to represent the special specifications of their wetlands and include specified local classes. These national terminologies are not understood internationally, and national classification systems lack sufficiency and flexibility when applied to a global scope (Scott & Jones, 1995). Ramsar convention recognized the need

for an international classification system for designated sites, to provide a basis for both local and international wetland inventories. This hierarchical classification system is based on the US classification system for deep water habitats and wetlands (Cowardin, 1979), which includes systems, subsystems, classes, and subclasses. Considering the limitations, in form of both quantity and quality of reference and earth observation data available for Iran, we followed the masterclasses suggested by the Ramsar convention to classify diverse wetland types founded in Iran (Fig. 2).

Materials and methods

Reference data

A variety of reliable sources were used to collect reference data for training and evaluating machine learning models. Collecting reference data with proper

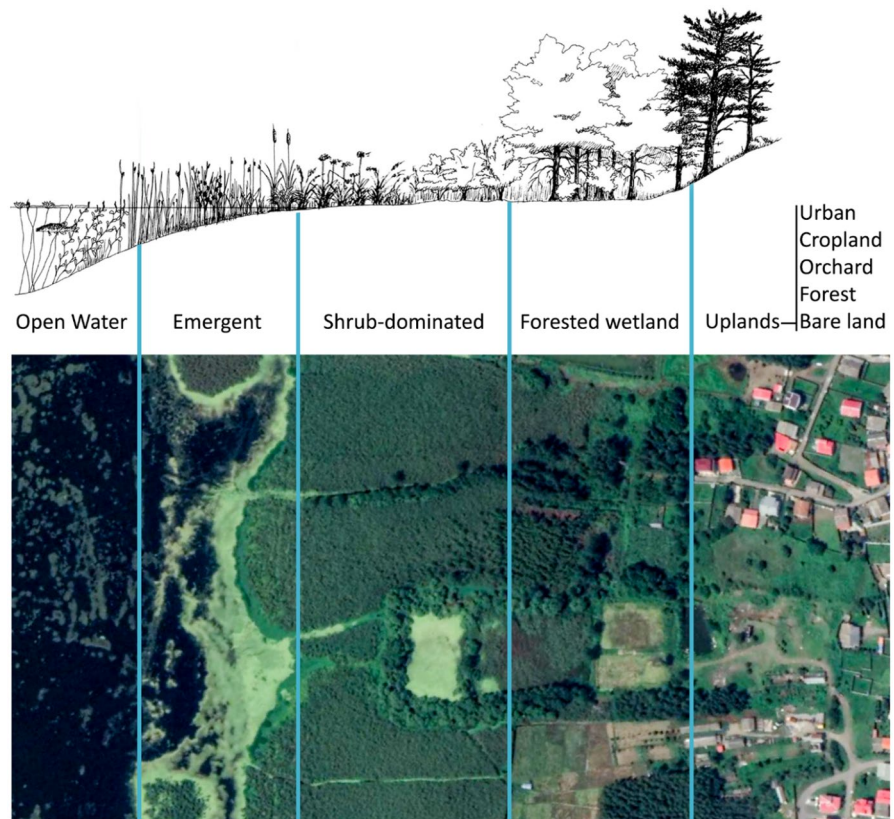
Table 1 List of Ramsar sites located in Iran

Ramsar Site No	Site name	Designation date	Area (ha)	Ramsar Criterion1	Wetland type	Montreux listed
49	Alagol, Ulmagol and Ajigol Lakes	1975–06-23	1400	Yes	Inland	No
47	Amirkelayeh Lake	1975–06-23	1230	Yes	Inland	No
40	Anzali Wetland Complex	1975–06-23	15,000	Yes	Inland, Marine, or coastal	Yes
46	Bujagh National Park	1975–06-23	3177	Yes	Inland, Marine, or coastal	No
1939	Choghakhor Wetland	2010–03-03	1687	No	Inland	No
52	Deltas of Rud-e-Gaz and Rud-e-Hara	1975–06-23	15,000	Yes	Inland, Marine, or coastal	No
51	Deltas of Rud-e-Shur, Rud-e-Shirin, and Rud-e-Minab	1975–06-23	45,000	Yes	Inland, Marine, or coastal	No
1308	Fereydoon Kenar, Ezbaran & Sorkh Ruds Ab-Bandans	2003–03-28	5427	No	Human-made	No
53	Gavkhouni Lake and marshes of the lower Zaindeh Rud	1975–06-23	43,000	Yes	Inland	No
1109	Gomishan Lagoon	2001–11-05	17,700	Yes	Marine or coastal	No
1006	Govater Bay and Hur-e-Bahu	1999–11-01	75,000	Yes	Inland, Marine, or coastal	No
44	Hamun-e-Puzak, south end	1975–06-23	10,000	Yes	Inland	Yes
42	Hamun-e-Saberi & Hamun-e-Helmand	1975–06-23	50,000	Yes	Inland	Yes
1940	Kanibarazan Wetland	2011–01-17	927	No	Inland	No
50	Khuran Straits	1975–06-23	100,000	Yes	Marine or coastal	No
48	Lake Gori	1975–06-23	120	Yes	Inland	No
43	Lake Kobi	1975–06-23	1200	Yes	Inland	No
37	Lake Parishan and Dasht-e-Arjan	1975–06-23	6200	Yes	Inland	No
38	Lake Urmia [or Orumiyeh]	1975–06-23	483,000	Yes	Inland	No
36	Miankaleh Peninsula, Gorgan Bay, and Lapoo-Zaghmarz Ab-bandan	1975–06-23	100,000	Yes	Inland, Marine or coastal, Human-made	No
39	Neiriz Lakes & Kamjan Marshes	1975–06-23	108,000	Yes	Inland, Marine, or coastal	Yes
41	Shadegan Marshes & mudflats of Khor-al Amaya & Khor Musa	1975–06-23	400,000	Yes	Inland, Marine, or coastal	Yes
1015	Sheedvar Island	1999–12-29	870	Yes	Marine or coastal	No
45	Shurgol, Yadegarlu & Dorgeh Sangi Lakes	1975–06-23	2500	No	Inland	Yes
2369	Zarivar	2016–07-17	2185.58	Yes	Inland	No

quality and quantity is often challenging in large-scale studies. A combination of office-based and field-work methods was used to obtain the data. Despite it is not the most cost-effective method, field data is considered the most reliable source of reference data,

especially in complex wetland habitats to determine the wetland types. Ramsar Site Information Service (<https://rsis.ramsar.org/> Accessed 9 January 2023) provides detailed information and reports about wetland types within Ramsar sites. This information is

Fig. 2 A classification scheme for Iran wetland mapping (high-resolution image of Anzali wetland complex from Google Earth and wetland cross-section from New England Wetland Plants, Inc.)



based on a field investigation from Ramsar Convention Monitoring Procedure. In addition, the Iranian Department of Environment provides geospatial information about both Ramsar sites and locally registered sites. These data are available in both formats of classified maps and reports.

To ensure the quality and consistency of reference data, office-based methods also were used. Some data were re-labeled and converted into the mentioned classification system to prevent inconsistency in form of different wetland descriptions and terminology. High-resolution images from Google Earth were used to update the borders of classes or to expand training samples. Also, Upland reference data was sampled from the national land cover provided by the Iranian Space Agency. The number of reference samples for each class is listed in Table 2 and the distribution of the test and train data is illustrated in Fig. 3.

Earth observation data and preprocessing

Different aspects of earth observation data are provided by the Sentinel mission from the Copernicus program under the management of the European Space Agency (ESA) in association with the European Commission. This constellation is consisting of both active and passive imaging instruments for atmospheric, land, and marine monitoring (Berger et al., 2012). Computational capability for large-scale studies, in addition to petabytes of earth observation data from various sources, is available through Google Earth Engine (GEE). Free access data from Sentinel missions in addition to robust cloud-computing platforms, like GEE, make unprecedented opportunities for monitoring wetlands and producing national wetland inventories. The spatial distribution of Sentinel-1 SAR and Sentinel-2 multispectral

Table 2 The number of polygons is used as training and testing data

Land cover	Train	Test	Total	Total area (km ²)
Water	181	84	265	326.11
Emergent	147	69	216	57.62
Shrub-dominated	205	86	291	44.44
Forested wetland	134	60	194	12.43
Cropland	163	76	239	104.82
Orchard	231	69	300	176.34
Urban	180	72	252	12.51
Forest	158	79	237	119.00
Bare land	349	155	504	1436.63
Total	1748	750	2498	2289.88

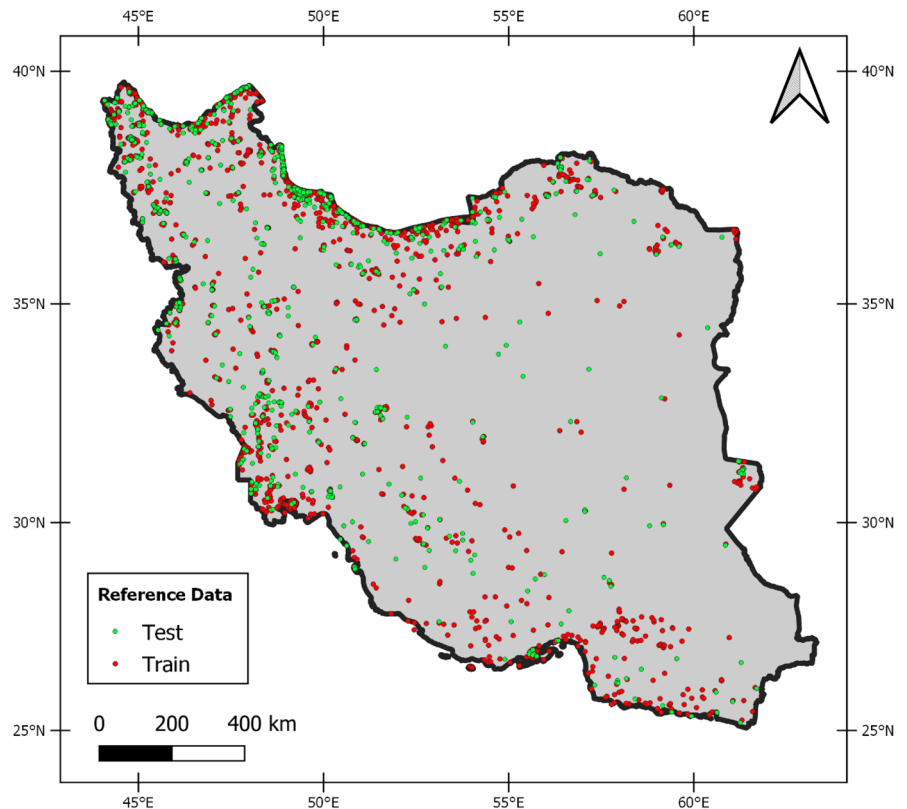
images, in addition to the Normalized Difference Vegetation Index (NDVI) index and topographic hill shade, is illustrated in Fig. 4.

In this study, we used a total of 1399 C-Band images from Sentinel-1 Synthetic Aperture Radar (SAR) from June to August 2020. This Level-1 10 m Ground Range Detected (GRD) data had a 250-km swath and was

collected in interferometric wide (IW) mode and was accessed from the GEE data catalog. The spatial scattering of Sentinel-1 images is illustrated in Fig. 3. Several preprocessing steps are already done for Sentinel-1 GRD images in GEE, including terrain correction, radiometric calibration, and noise removal. In addition to these, a 7×7 adaptive sigma Lee filter has been applied to reduce speckle noises and SAR backscatter coefficient σ^0 (Sigma Naught), and other derivatives of these values were extracted (Table 3). Each polarization component is sensitive to specified characteristics of wetlands. Specifically, herbaceous wetland classes with sparse canopy closure are better discriminated in σ^0_{VV} observations are useful.

With a joined 5-day revisit time, Sentinel-2A and Sentinel-2B provide a high spatial resolution and wide-swath dataset for monitoring wetlands. In this study, a total number of 5839 Level-2A surface reflectance data with less than 20% cloud coverage were used. To minimize the cloud coverage and dynamic characteristics of wetlands, a tri-monthly summer timeframe from June to August 2020 was used to filter the data and create a median summer composite image. To remove

Fig. 3 Distribution of the train and test polygon centroids across the study area



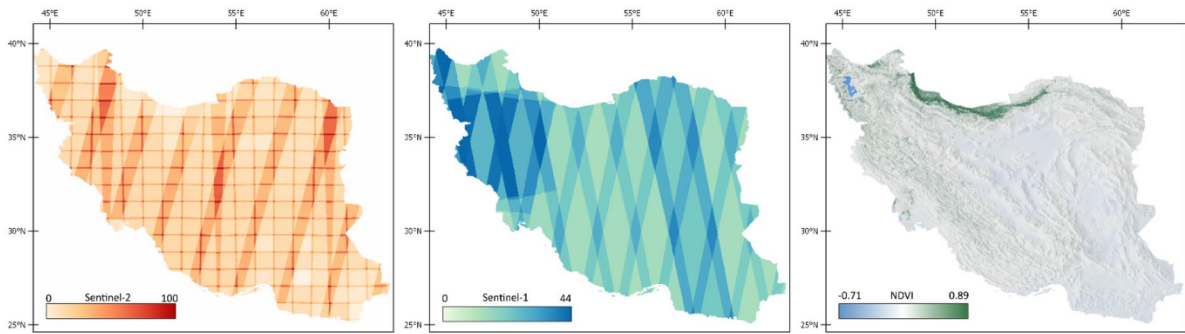


Fig. 4 NDVI index on hill shade map of Iran and data distribution for Sentinel-1 SAR and Sentinel-2 spectral data

the remaining clouds and cirrus, the QA60 bitmask band from Sentinel-2 metadata was used. In addition, a thresholding method was used on the Sentinel-2 Aerosol band to remove other clouds and aerosols. To produce a high-resolution national wetland inventory, only four spectral bands (RGB and NIR bands) with 10 m resolution were used. In addition to spectral bands, a list of spectral features from Sentinel-2 and topographic features from the Shuttle Radar Topography Mission (SRTM) were extracted (Table 3).

Classification scheme

In this study, we used an object-based image analysis (OBIA) framework (Mahdianpari et al., 2020a, b) and the flowchart of different processing stages is shown in Fig. 5. This framework is containing a simple

non-iterative clustering method and a Random Forest (RF) classifier. Iran consists of different wetland classes with unique characteristics. This variation is in the light of different climate conditions, influenced by Iran’s location between the subtropical humidity of the eastern Mediterranean areas and the aridity of the Arabian Desert areas. To increase the commonality between wetland vegetation classes, the classification system was applied separately for four major sections of the study area (Mahdianpari et al., 2020a, b). We derived these sections by joining regions from ecological zones (subtropical humid forest, mountains system, steppe, and desert), climate classification maps (Koeppen–Geiger classification), and provincial zones to minimize variation in each section, in terms of climate, temperature, precipitation, soil, vegetation, landform, and human activities.

Table 3 List of features extracted from different datasets

Data	Feature description	Formula
Sentinel-1	Vertically transmitted and received SAR backscattering coefficient	σ_{VV}^0
	Vertically transmitted, horizontally received SAR backscattering coefficient	σ_{VH}^0
	Span or total scattering power	$ \sigma_{VV}^0 + \sigma_{VH}^0 $
	Ratio	$ \sigma_{VV}^0 ^2 + \sigma_{VH}^0 ^2$
Sentinel-2	Spectral bands Blue (B2), Green (B3), Red (B4), NIR (B8)	
	The Normalized Difference Vegetation Index (NDVI)	$(\text{NIR} - \text{Red}) / (\text{NIR} + \text{Red})$
	The Normalized Difference Water Index (NDWI)	$(\text{Green} - \text{NIR}) / (\text{Green} + \text{NIR})$
	Green Chlorophyll Vegetation Index (GCVI)	$(\text{NIR} / \text{Green}) - 1$
	Green Normalized Difference Vegetation Index (GNDVI)	$(\text{NIR} - \text{Green}) / (\text{NIR} + \text{Green})$
SRTM DEM	Ratio Vegetation Index (RVI)	NIR / Red
	Elevation	
	Slope	
	Aspect	

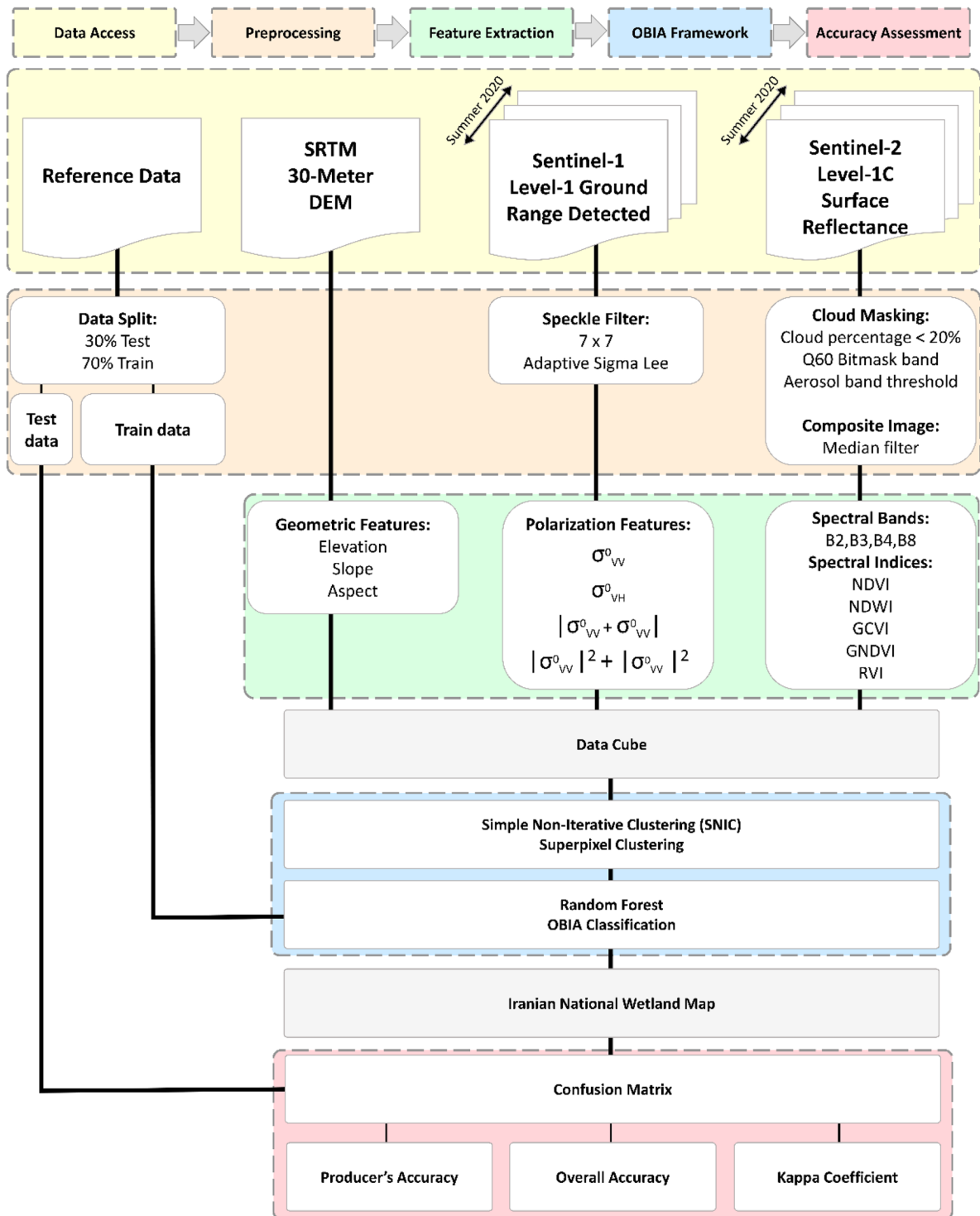


Fig. 5 The flowchart of Iranian wetland mapping processing stages

Within a given neighborhood, the OBIA approach uses contextual information and does not have salt and pepper noises caused by conventional pixel-based approaches. Superpixel segmentation was applied by using the simple non-iterative clustering (SNIC) algorithm (Achanta & Susstrunk, 2017). By using color and spatial coordinates distance in five-dimensional space, this algorithm starts by measuring the dependency of the central pixel on a regular grid (Achanta & Susstrunk, 2017). As a non-parametric classifier, RF shows promising results in remote sensing fields, and it is superior to some other well-known classifiers (Sheykhmousa et al., 2020). Compared to support vector machine (SVM), RF is easily tunable and has better performance in comparison to decision tree (DT). By using random samples from training data, an ensemble decision tree is created by RF with bootstrap aggregating (bagging approach), and the correlation between the trees is minimized by specifying the finest splitting of the nodes (Breiman, 2001). RF requires two adjustable parameters, the number of variables (*Mtry*) and the number of trees (*Ntree*). Specifically, the square root of the number of variables was used for *Mtry* and a total number of 500 for *Ntree*. These parameters were adjusted based on a trial-and-error procedure and previous studies on the classification of wetlands (Mahdianpari et al., 2019, 2020a, b). All the OBIA steps were applied in the GEE and the models in each zone were trained with almost 70% of the reference data. Evaluation of the produced maps is a key element in land cover mapping with earth observation data. Approximately, 30% of the reference data were used as independent testing data for accuracy assessment.

Results

Figure 6 illustrates the nationwide wetland inventory map produced by object-based RF classification at 10-m spatial resolution. All these image datasets and products can be downloaded from rslab.ut.ac.ir (Accessed 9 January 2023). A significant proportion of Iran's land cover is covered with bare land classes, such as clay, sands, salty lands, and outcrops, which are not subject to interest in this article.

Lake Urmia, registered as a national park and recorded as the biggest water body in Iran, is illustrated in Fig. 6A This hypersaline lake is fed by streams,

rainfalls, and springs, and also extensive brackish marshes surround it. The water content of this lake is dependent on seasonal variations in salinity and water level. Also, a road bridge connects two sides of this lake. Figure 6B is the results from Anzali Wetland Complex, a permanently flooded wetland surrounded by water impoundments that are fringed by damp grasslands, reedbeds, and seasonally flooded marshes. A dune system separates this large, freshwater lagoon from the sea, which is supporting extensive floating vegetation, abundant submerged, and reedbeds, and is fed by several rivers. Wintering, Staging, and breeding of water birds made this wetland site internationally important. Because of changes in the level of water and incensement of nutrient enrichment, this site is listed in Montreux Record. This area contains a rich vegetation variety due to high precipitation and includes heterogeneous wetland classes and agriculture areas.

Miankaleh Peninsula and Gorgan Bay (Fig. 6C) is a brackish bay that is almost entirely disconnected from the Caspian Sea. This freshwater lagoon supports seasonally flooded woodland, extensive reedbeds, and also freshwater marshes. This wetland ecosystem is intensely significant for the wintering waterbirds, especially for their passage, breeding, and nesting. Ajjgol and Ulmagol are seasonally filled freshwater lakes, depicted in Fig. 6C Precipitation in autumn and winter feeds these lakes, and in drought periods, they become desiccated. Alagol, also, is moderately saline and is fringed by grass marshes and reeds. Due to the high rate of wildfowl hunters' disturbance and the water extraction for irrigation purposes, these lakes are on the Montreux Record.

Figure 6D shows the Zarivar freshwater wetland, fed mostly by lake floor springs and located at the foot of the Zagros Mountain system. Relatively extensive reed beds make this wetland area the habitat for a lot of species, and the local societies near the Zarivar lake depend on it for recreational activities and fishing. The Hawizeh Marsh is a wetland site located at the border of Iran and Iraq (Fig. 6F). Since the 1990s, dam-building activities, as well as warfare destruction, are seen as the main expected dangers to the site. Also, recent oil developments in surrounding regions threaten to prevent the recovery and restoration of the marshes and affect the natural environment.

Khuran Straits (Fig. 6G) is an extensive intertidal silt flat including mangrove forests (Hara forests), plenty of estuarine creeks, islands, and salt marshes. Brown and

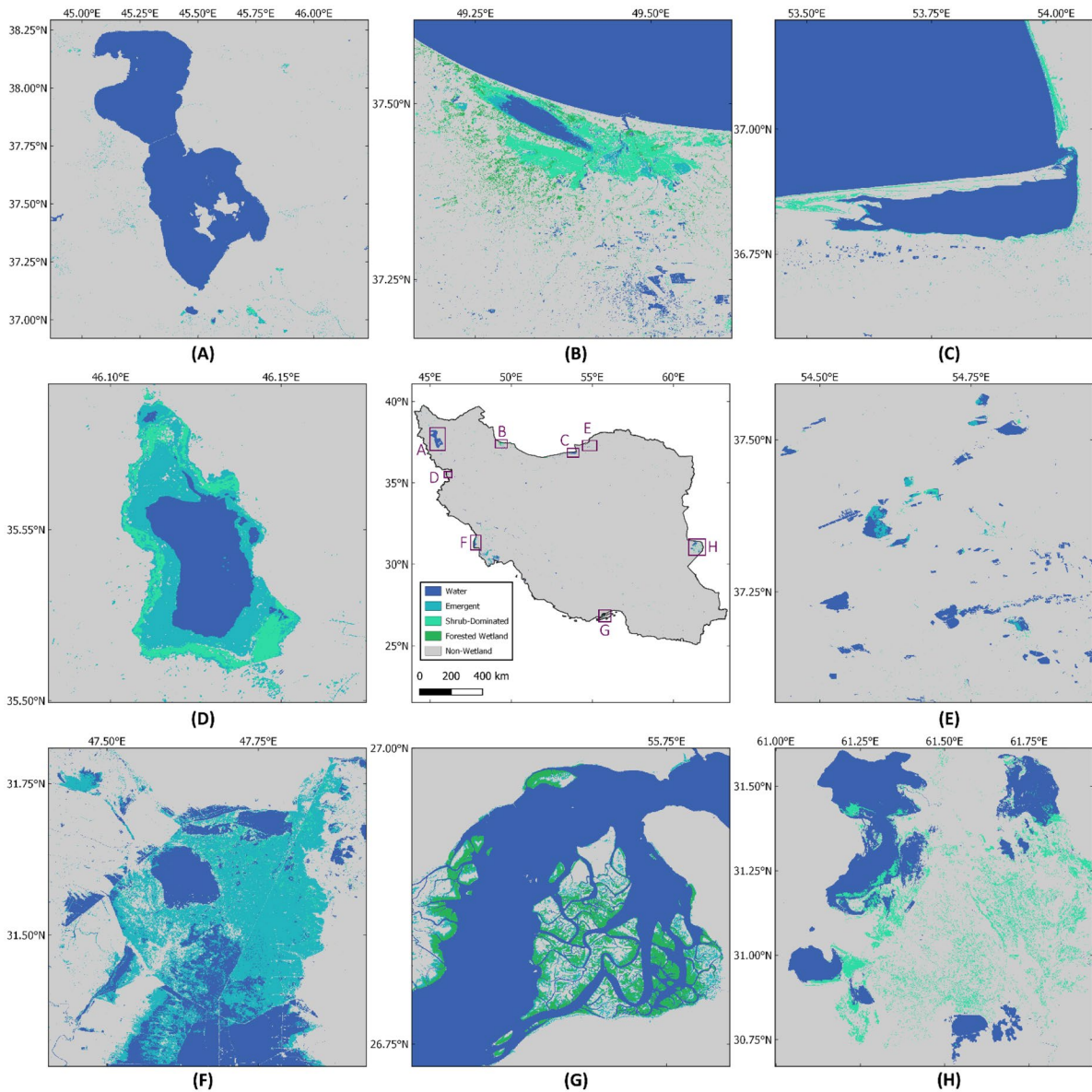


Fig. 6 The nationwide wetland inventory map for Iran and subsets from Ramsar sites. **A** Lake Urmia; **B** Anzali Wetland Complex; **C** Miankaleh Peninsula and Gorgan Bay; **D** Zarivar;

E Alagol, Ulmagol, and Ajigol Lakes; **F** Hawizeh Marsh; **G** Khuran Straits (Hara mangrove forests); and **H** Hamun-e-Saberi and Hamun-e-Helmand

red algae growth are supported by shallow saline waters and habitat for crustaceans is provided by the intertidal mangroves. A closed drainage basin is shown in Fig. 6H and contains two predominantly shallow freshwater lakes and associated wetland areas, located at the border of Iran and Afghanistan. This site is listed on the Montreux Record due to river control structures, drought, and increasing stress from crop irrigation and urbanization.

Figure 7 shows detailed levels of classification from three Ramsar Sites. All the results are visually compared with the latest Iran land cover map (Ghorbanian et al., 2020) and high-resolution images from ESRI. Generally, there is an agreement and correlation between the produced results in this article and results from previous land cover maps. However, the wetland classes from previous maps are limited and did not separate wetland

vegetation, especially in heterogeneous areas. For example, the first row of Fig. 7 shows the successful separation of floating emergent from upper shrub-dominated areas. Also in the second row, wetland classes are mixed with water bodies, and both floating shrublands and emergent are identified. In the third row, a typical sequence of wetland vegetation classes occurred at the

Zarivar lake, floating emergent vegetation is separated from more stable shrub-land areas.

The confusion matrix of the four different ecological zones is illustrated in Fig. 8. Columns of the confusion matrix show the predicted values, and the rows show the actual values from the ground truth data. The confusion matrix shows the performance of the

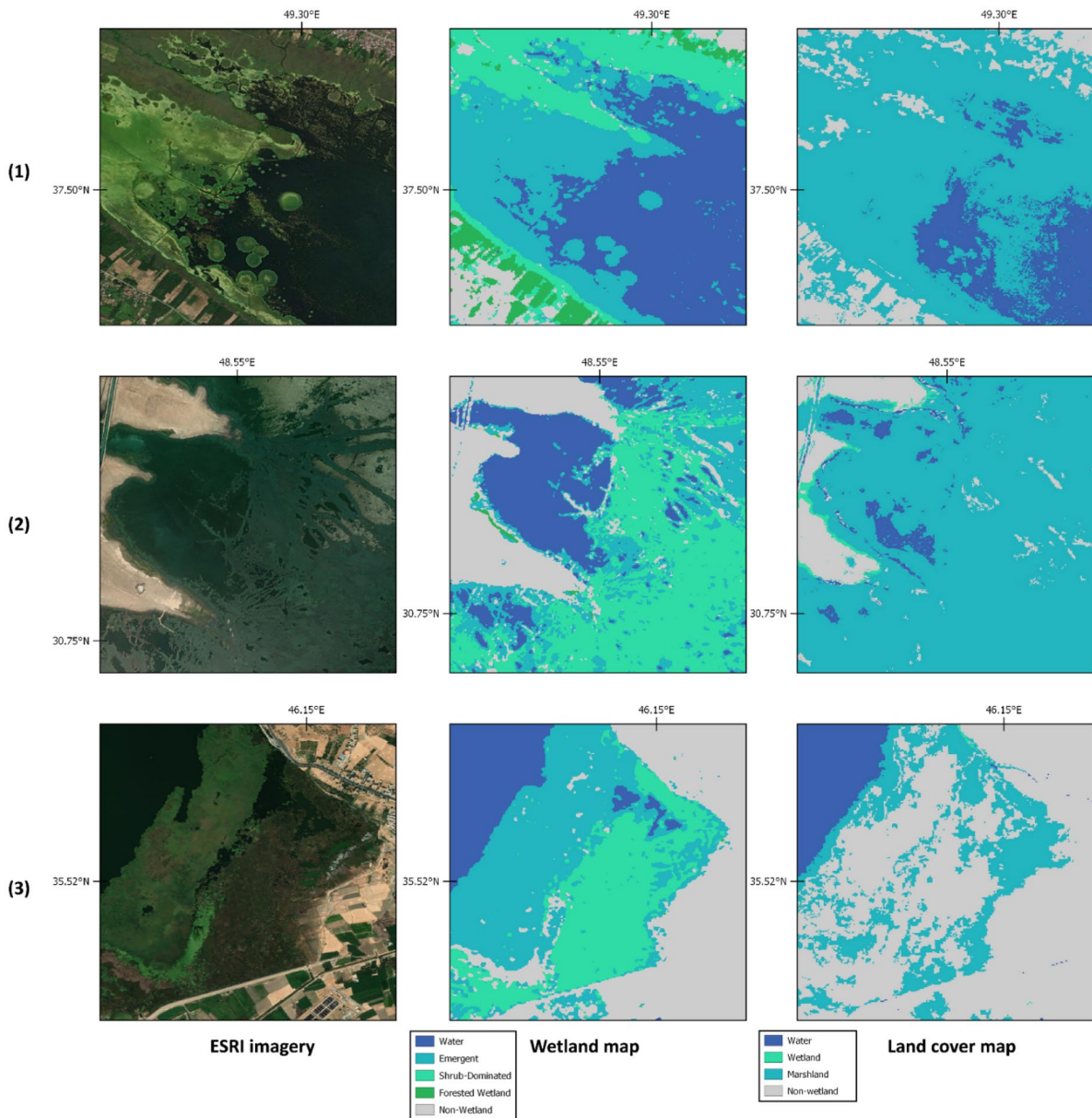


Fig. 7 Subsets from ESRI high-resolution images, Iranian wetland map, and land cover map from 1) Anzali Wetland Complex, (2) Shadegan Marshes, and (3) Zarivar Lake

OBIA classification results in different classes and the number of samples that were misclassified into other classes in each region.

The final map was produced with an overall accuracy of 96.39%. The producer’s accuracy of wetland classes is shown in Fig. 9. From wetland classes, Water had the highest accuracy due to its special characteristics in both spectral and radar datasets. Shrub-dominated and emergent areas also had promising accuracy ranging from 86.46 to 99% for Shrub-dominated and 82.40 to 95.34% for emergent, showing great separation of these two heterogeneous wetland vegetation areas. Forested

wetlands had 64.91 to 99.25% producer accuracy. This variation is in the light of dense forest systems in the humid forest ecological zone which is misclassified with forested wetlands and mangroves in the southern Steppe ecological zone, which are easily distinguished from surrounding waters. Having an arid climate, the desert zone did not include emergent and forested wetland classes. Among upland classes, bare land areas cover most of our study area and had the highest accuracy. However, urban areas, especially in southern steppe and desert zones with dry climates, are usually misclassified with bare lands, on account of nearly similar spectral

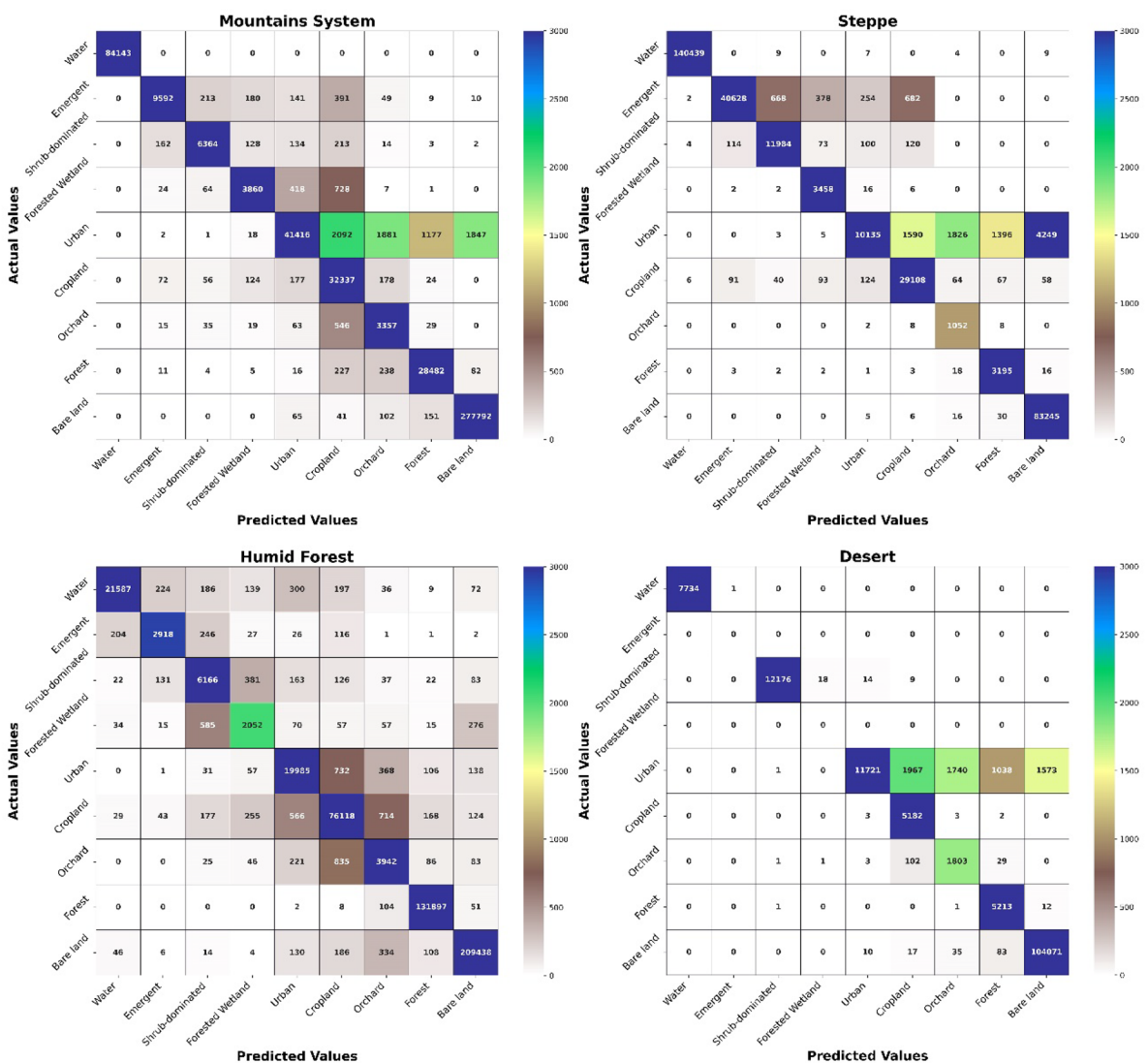


Fig. 8 Confusion matrix of the different ecological zones

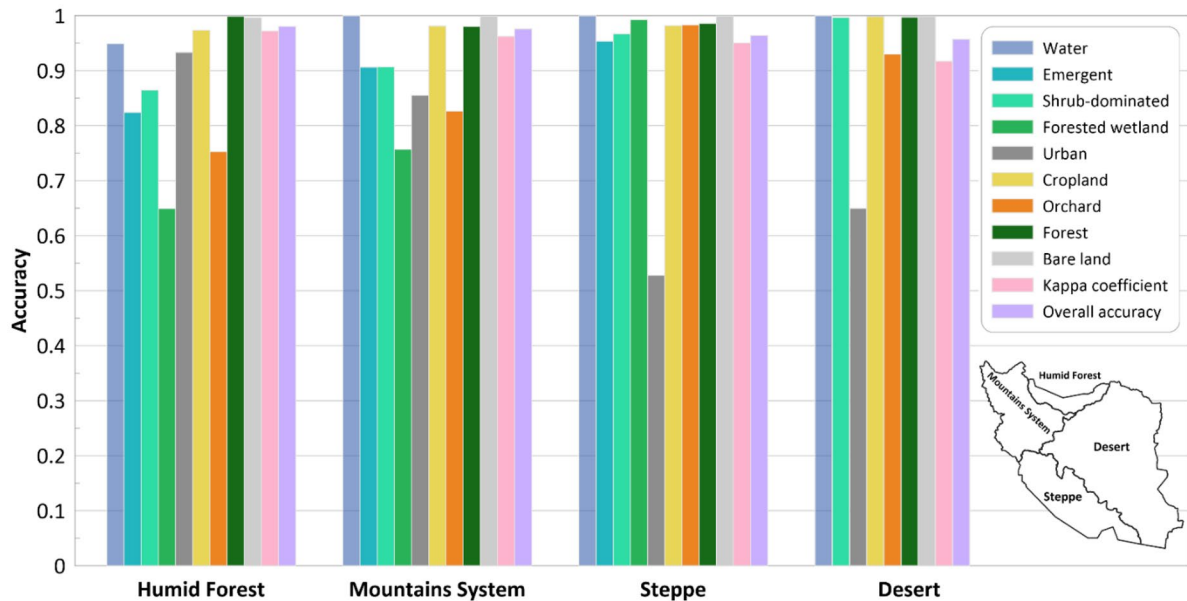


Fig. 9 Producer's accuracy of different wetland classes and kappa coefficient from different ecological regions

characteristics. Cropland and orchard classes, corresponding to agricultural areas, had an accuracy range between 75.25 and 98%. Producer's accuracy for the forest class was above 95%, and the kappa coefficient ranged from 0.91 to 0.97 for all regions.

The proportion of each class, with the exclusion of bare land and urban classes due to unbalance coverage, is illustrated in Fig. 10 for study area regions with an explosion of wetland classes. Generally, forest and cropland classes cover more area than wetland classes. Rain forests are the major land cover in the northern humid forest area. The existence of Urmia Lake and Hur al-Azim in the mountain system and southern steppe region increased the proportion of water bodies in these areas. Among wetland vegetation classes, the shrub-dominated class covers the most area. On the other hand, forested wetland areas are rare wetland classes in Iran, only existing in the southern part of Iran as mangroves and partial coverage in northern and northern western areas.

The area of different wetland classes, calculated from the Iranian wetland inventory, is depicted in Fig. 11. Wetland classes, including water bodies, cover around 22,384.591 km² in Iran. In comparison to the Ramsar report, which is 14886.24 km² for registered sites, this estimation is respectively acceptable because all local and small wetland classes, in

addition to small water bodies, streams and rivers, are mapped in this study. Both emergent and shrub-dominated areas cover about 3405.96 km². Forested wetland areas only cover 709.54 km², representing the rare wetland class.

The binary mask of wetland classes, in addition to other vegetation classes (forest, cropland, orchard), is illustrated in Fig. 12. Wetlands and water bodies only cover around 1.35% of Iran's area. Iran is facing critical water resource problems due to frequent recent droughts and overconsumption of both groundwater and surface water sources. Unfortunately, drying wetlands, lakes, and rivers, in addition to desertification, soil erosion, land subsidence, and declining groundwater levels, are consequences of this water crisis. The absence of a far-reaching comprehension of the main drivers of the issue, in addition to the lack of sustainable structure of the water management system in Iran, does not provide a basis for developing long- and short-term solutions to Iran's water problems. Providing a national wetland inventory may be one of the first steps toward addressing these issues. High-resolution mapping and monitoring of heterogeneous and complex wetland sites are advantageous for understanding cyclic land cover transition in wetland-dominated areas. Up-to-date information about wetland sites, especially about the location, extent, and water content of these areas, is crucial

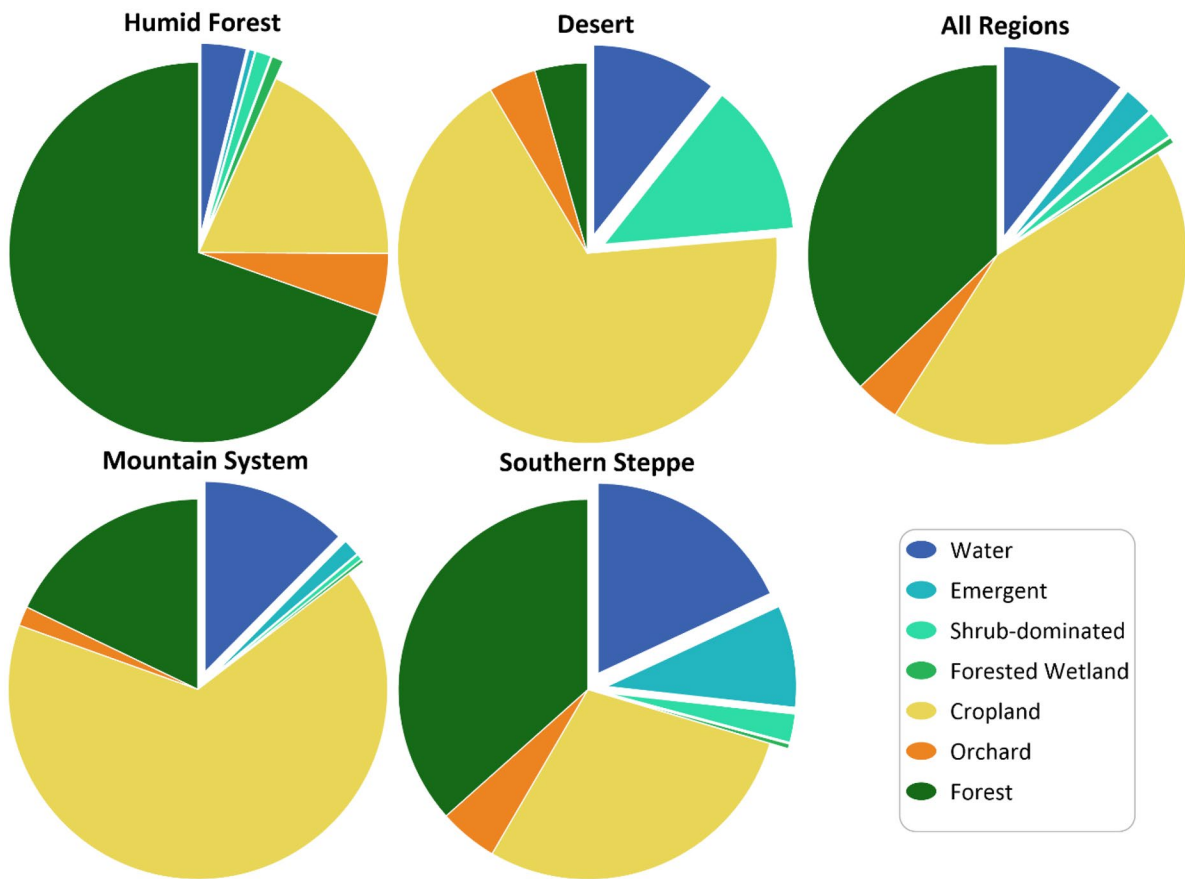


Fig. 10 The percentage of each class in different ecological zones. Urban and bare land classes are excluded

for the restoration and conservation of these valuable ecosystems. The special opportunity for precise monitoring and mapping of wetland environments on previously infeasible spatial and temporal scales is provided by recently developed high temporal and spatial resolution open-access earth observation data, in addition to cloud computation platforms.

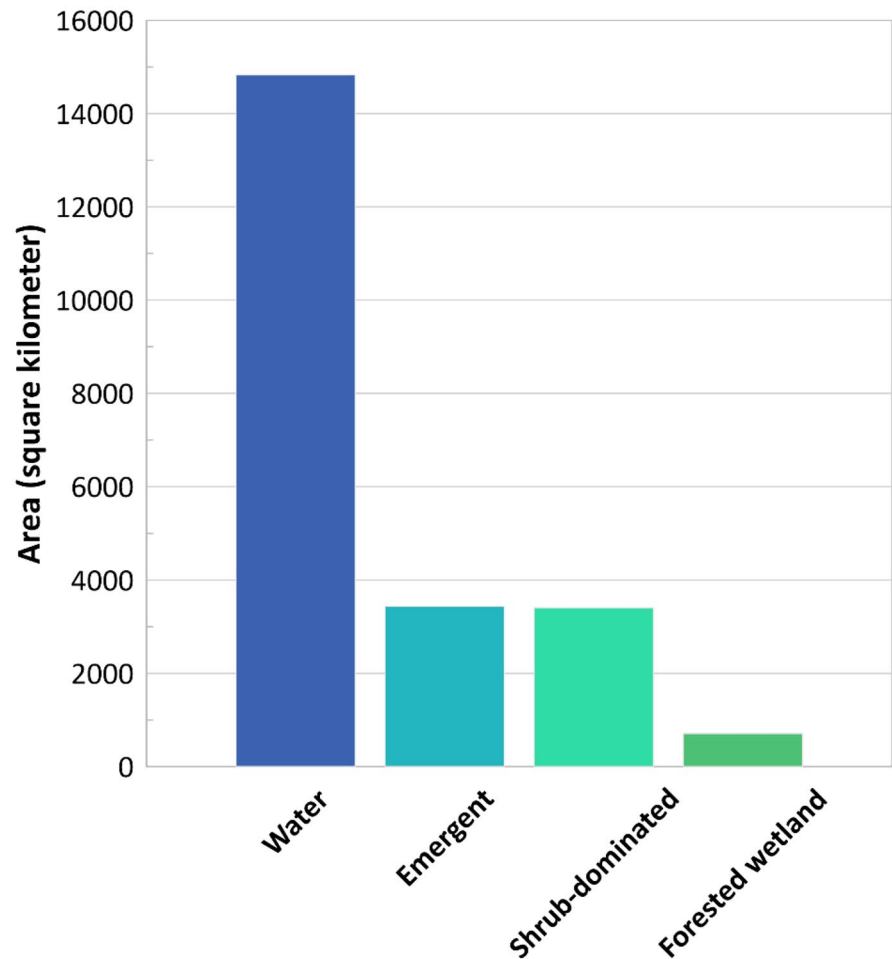
Discussion

Leveraging cloud massive computational power and storage capacity, an Iran-wide wetland map was produced that is more advanced compared to old-fashioned approaches, such as the interpretation of aerial photography and small-scale wetland inventories. These generalized maps are especially interesting in various applications, demanding wetland information and regional land cover maps for decision-making,

reporting purposes, and modeling (Ashraf et al., 2021). Compared with other similar sentinel-based national and continental scale wetland inventories, the 96% overall accuracy of the resulting map is acceptable (Mahdianpari et al., 2021; Venter & Sydenham, 2021). The resulting maps and high accuracy demonstrate the capabilities of the OBIA classification method and RF classifier. However, recent advances in deep learning approaches for wetland mapping have shown promising results for more advanced classification systems and better separation of wetland classes in homogeneous areas (Hosseiny et al., 2022). The quality of deep learning approaches is highly dependent on the amount of the available reference data, and implementation of them for large-scale areas is still challenging due to the computational sources required for training the model and high-density field data across the study area.

Previous wetland mapping studies in Iran focused on single wetland sites and lacked spatial coverage

Fig. 11 The area regarding each wetland class



of the produced map, in addition to the advanced classification system (Kharazmi et al., 2018; Minaei & Kainz, 2016; Qureshi et al., 2020). Due to a lack of previous nationwide wetland inventory for Iran, a direct comparison was not possible. However, the total area of the wetland classes identified in this study showed general agreement with the previous Ramsar reports (Ramsar Convention, 2016) and general land cover maps (Ghorbanian et al., 2020). It is worth mentioning that the production of wetland inventories is more challenging than general land cover maps due to the fact that spectral responses of wetland classes are closer, especially in homogenous wetland areas, rather than general land cover classes (e.g., bare land, cropland, and open water).

The usage of auxiliary data besides spectral and SAR data for wetland mapping has been demonstrated in previous studies. In particular, Mahdianpari et al.

(2021) enhanced the previous existing wetland inventories of Canada by using temperature, precipitation and the Visible Infrared Imaging Radiometer Suite (VIIRS) day and night band. Unfortunately, due to data gaps and the unavailability of the mentioned auxiliary data in the GEE for Iran, usage of them is not applicable. Besides Sentinel platforms, Landsat data have been used for wetland mapping at lower spatial resolution (Mao et al., 2020). The usage of Landsat data decreases the spatial resolution of wetland maps. However, monitoring long-term wetland changes is only possible with the science-grade archive of Landsat data for the past 50 years (Kouhgard et al., 2022). With the availability of open-access Landsat archive, there have been studies on regional and national wetland changes internationally (Amani et al., 2022; Hopkinson et al., 2020) and in Iran (M. Hemati et al., 2022; Qureshi et al., 2020). However, Iranian wetland

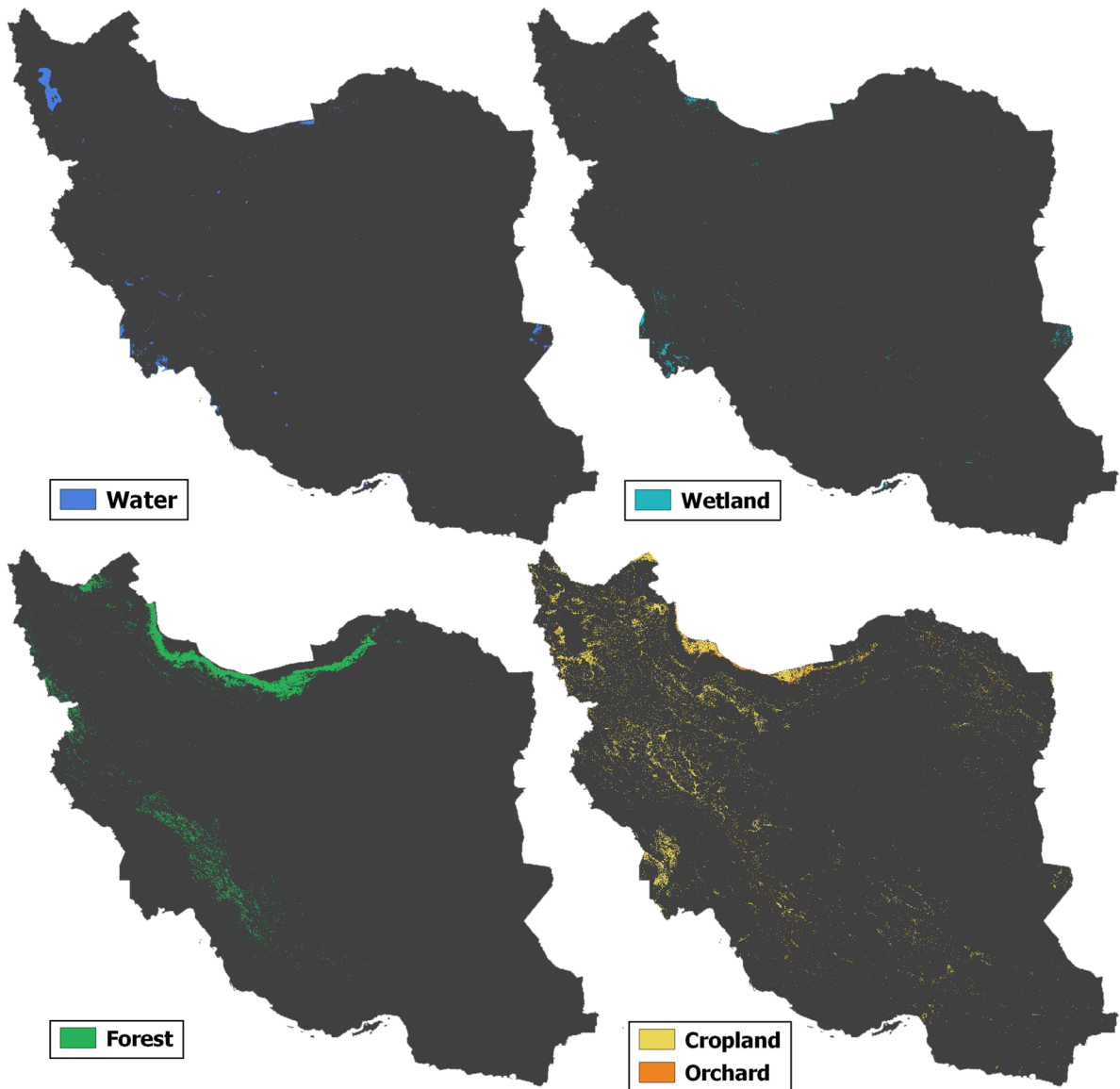


Fig. 12 Binary mask of water bodies, wetlands, forests, and agriculture classes in Iran

change detection studies were limited to a small scale or lacked the inclusion of wetland classes. Monitoring wetland changes in different classes require historical reference data, which are not mostly available. Another approach would be releasing updates of the current wetland inventories, with up-to-date ground truth and enhancement in classification. Future studies can use the produced 10-m wetland inventories with wetland sub-classes as the reference for future change detections.

Conclusion

Monitoring and mapping the wetland areas has been a challenging task, especially at national-scale, due to time and budget requirements for field data collection, the fuzziness of boundaries between wetland classes, and the diversity of wetland types in Iran, in addition to the huge amount of storage and computational power required to process geospatial big-data. Nevertheless, recent advances in satellite imagery,

such as accessibility of free and high-resolution optical and radar data, as well as powerful online computing platforms with petabytes of various earth observation data and massive computation power that bring state-of-the-art algorithms to the data, offer unprecedented opportunities for mapping these important natural resources. By using the unmatched computational capabilities of GEE and through the fusion of radar and spectral data to benefit from both data sources in a large-scale investigation, we produced a 10-m Iran national wetland inventory using a mixture of Sentinel-1 SAR and Sentinel-2 multispectral data. A classification system was developed and adapted from Ramsar wetland types, to be suitable to cover the diversity of Iranian wetlands, as well as different upland classes. An object-based image analysis technique was implicated in this study, including SNIC superpixel clustering and a Random Forest classifier. A separate classification was performed for each of the four ecological zones, and through the evaluation step, the overall accuracy of all zones ranges from 95 to 98%. The accuracy of the results matches with similar sentinel-based studies in other countries and visual comparison with the existing land cover maps shows the general agreement between the produced wetland inventory and general land cover maps. Among nine classes, water achieved the highest producer's accuracy and shrub-dominated and emergent classes range from 82.4 to 99%. Forested wetland, as the rarest wetland class in Iran, ranges from nearly 65 to 98% producer's accuracy. Wetland classes, which are more complicated to classify than the general land cover classes, were identified in this study with acceptable accuracy, and the final map was produced with the wetland classification system that was not studied in Iran before.

In this study, we estimated that 22,384.591 km² of Iran are covered with wetland classes and water bodies. The estimated area shows the agreement from previous Ramsar and national land cover maps, with the advantage of the inclusion of various wetland classes and local wetland sites. Also, the distribution of water bodies, wetland classes, and other vegetation areas are highlighted in this study. Importantly, unprecedented information about the spatial distribution, status, and extent of wetlands classes have been provided by the resulting Iranian wetland inventory map and, therefore, are useful for both governmental and commercial sections, including environmental

consultants, federal and provincial governments, and municipalities. Produced wetland inventory at 10-m spatial resolution can be used as the base maps for future change detection or wetland inventory updates.

Author contribution Conceptualization: M.A.H., M.H., and M.M. Methodology: M.A.H. Writing original draft preparation: M.H. and M.M. Writing review and editing: M.H., F.M., M.H., and M.M. Visualization: M.A.H., M.H., and F.M. Supervision: M.H. and M.M. All authors have read and agreed to the published version of the manuscript.

Availability of data and material Publicly available datasets were analyzed in this study. These datasets can be found here: <https://rslab.ut.ac.ir/>.

Code availability Not applicable.

Declarations

Conflict of interest The authors declare no competing interests.

References

- Achanta, R., & Susstrunk, S. (2017). Superpixels and polygons using simple non-iterative clustering. In *2017 IEEE Conference on Computer Vision and Pattern Recognition (CVPR)* (pp. 4895–4904). Presented at the 2017 IEEE Conference on Computer Vision and Pattern Recognition (CVPR), Honolulu, HI: IEEE. <https://doi.org/10.1109/CVPR.2017.520>
- Adam, E., Mutanga, O., & Rugege, D. (2010). Multispectral and hyperspectral remote sensing for identification and mapping of wetland vegetation: A review. *Wetlands Ecology and Management*, *18*(3), 281–296. <https://doi.org/10.1007/s11273-009-9169-z>
- Alibakhshi, S., Groen, T. A., Rautiainen, M., & Naimi, B. (2017). Remotely-sensed early warning signals of a critical transition in a wetland ecosystem. *Remote Sensing*, *9*(4), 352. <https://doi.org/10.3390/rs9040352>
- Amani, M., Kakooei, M., Ghorbanian, A., Warren, R., Mahdavi, S., & Brisco, B., et al. (2022). Forty years of wetland status and trends analyses in the Great Lakes using Landsat archive imagery and Google Earth Engine. *Remote Sensing*, *14*(15), 3778. <https://doi.org/10.3390/rs14153778>
- Amani, M., Salehi, B., Mahdavi, S., Granger, J. E., Brisco, B., & Hanson, A. (2017). Wetland classification using multi-source and multi-temporal optical remote sensing data in Newfoundland and Labrador. *Canada. Canadian Journal of Remote Sensing*, *43*(4), 360–373. <https://doi.org/10.1080/07038992.2017.1346468>
- Ashraf, S., Nazemi, A., & AghaKouchak, A. (2021). Anthropogenic drought dominates groundwater depletion in Iran. *Scientific Reports*, *11*(1), 9135. <https://doi.org/10.1038/s41598-021-88522-y>
- Berger, M., Moreno, J., Johannessen, J. A., Levelt, P. F., & Hanssen, R. F. (2012). ESA's sentinel missions in

- support of Earth system science. *Remote Sensing of Environment*, 120, 84–90. <https://doi.org/10.1016/j.rse.2011.07.023>
- Blaschke, T. (2010). Object based image analysis for remote sensing. *ISPRS Journal of Photogrammetry and Remote Sensing*, 65(1), 2–16. <https://doi.org/10.1016/j.isprsjprs.2009.06.004>
- Breiman, L. (2001). Random forests. *Machine Learning*, 45(1), 5–32. <https://doi.org/10.1023/A:1010933404324>
- Chopra, R., Verma, V. K., & Sharma, P. K. (2001). Mapping, monitoring and conservation of Harike wetland ecosystem, Punjab, India, through remote sensing. *International Journal of Remote Sensing*, 22(1), 89–98. <https://doi.org/10.1080/014311601750038866>
- Corcoran, J. M., Knight, J. F., & Gallant, A. L. (2013). Influence of multi-source and multi-temporal remotely sensed and ancillary data on the accuracy of random forest classification of wetlands in Northern Minnesota. *Remote Sensing*, 5(7), 3212–3238. <https://doi.org/10.3390/rs5073212>
- Cowardin, L. M. (1979). *Classification of wetlands and deep-water habitats of the United States*. Fish and Wildlife Service, US Department of the Interior.
- Cox, C. (1992). Satellite imagery, aerial photography and wetland archaeology: An interim report on an application of remote sensing to wetland archaeology: The pilot study in Cumbria. *England. World Archaeology*, 24(2), 249–267. <https://doi.org/10.1080/00438243.1992.9980206>
- Daboor, M., White, L., Brisco, B., & Charbonneau, F. (2015). Change detection with compact polarimetric SAR for monitoring wetlands. *Canadian Journal of Remote Sensing*, 41(5), 408–417. <https://doi.org/10.1080/07038992.2015.1104634>
- Durieux, L., Kropáček, J., de Grandi, G. D., & Achard, F. (2007). Object-oriented and textural image classification of the Siberia GBFM radar mosaic combined with MERIS imagery for continental scale land cover mapping. *International Journal of Remote Sensing*, 28(18), 4175–4182. <https://doi.org/10.1080/01431160701236837>
- Gallant, A. L., Kaya, S. G., White, L., Brisco, B., Roth, M. F., Sadinski, W., & Rover, J. (2014). Detecting emergence, growth, and senescence of wetland vegetation with polarimetric synthetic aperture radar (SAR) data. *Water*, 6(3), 694–722. <https://doi.org/10.3390/w6030694>
- Gessner, U., Machwitz, M., Esch, T., Tillack, A., Naeimi, V., Kuenzer, C., & Dech, S. (2015). Multi-sensor mapping of West African land cover using MODIS, ASAR and TanDEM-X/TerraSAR-X data. *Remote Sensing of Environment*, 164, 282–297. <https://doi.org/10.1016/j.rse.2015.03.029>
- Ghimire, B., Rogan, J., & Miller, J. (2010). Contextual land-cover classification: Incorporating spatial dependence in land-cover classification models using random forests and the Getis statistic. *Remote Sensing Letters*, 1(1), 45–54. <https://doi.org/10.1080/01431160903252327>
- Ghorbanian, A., Kakooei, M., Amani, M., Mahdavi, S., Mohammadzadeh, A., & Hasanlou, M. (2020). Improved land cover map of Iran using Sentinel imagery within Google Earth Engine and a novel automatic workflow for land cover classification using migrated training samples. *ISPRS Journal of Photogrammetry and Remote Sensing*, 167, 276–288. <https://doi.org/10.1016/j.isprsjprs.2020.07.013>
- Grenier, M., Labrecque, S., Garneau, M., & Tremblay, A. (2008). Object-based classification of a SPOT-4 image for mapping wetlands in the context of greenhouse gases emissions: The case of the Eastmain region, Québec, Canada. *Canadian Journal of Remote Sensing*, 34(sup2), S398–S413. <https://doi.org/10.5589/m08-049>
- Guo, L., Chehata, N., Mallet, C., & Boukir, S. (2011). Relevance of airborne lidar and multispectral image data for urban scene classification using Random Forests. *ISPRS Journal of Photogrammetry and Remote Sensing*, 66(1), 56–66. <https://doi.org/10.1016/j.isprsjprs.2010.08.007>
- Hemati, M. A., Hasanlou, M., Mahdianpari, M., & Mohammadimanesh, F. (2021a). Wetland mapping of northern provinces of Iran using Sentinel-1 and Sentinel-2 in Google Earth Engine. In *2021a IEEE International Geoscience and Remote Sensing Symposium IGARSS* (pp. 96–99). Presented at the IGARSS 2021a - 2021a IEEE International Geoscience and Remote Sensing Symposium, Brussels, Belgium: IEEE. <https://doi.org/10.1109/IGARSS47720.2021.9554984>
- Hemati, M., Hasanlou, M., Mahdianpari, M., & Mohammadimanesh, F. (2021b). A systematic review of Landsat data for change detection applications: 50 years of monitoring the earth. *Remote Sensing*, 13(15), 2869. <https://doi.org/10.3390/rs13152869>
- Hemati, M., Mahdianpari, M., Hasanlou, M., & Mohammadimanesh, F. (2022). Iranian wetland hydroperiod change detection using an unsupervised method on 20 years of Landsat data within the Google Earth Engine. In *IGARSS 2022 - 2022 IEEE International Geoscience and Remote Sensing Symposium* (pp. 6209–6212). Presented at the IGARSS 2022 - 2022 IEEE International Geoscience and Remote Sensing Symposium, Kuala Lumpur, Malaysia: IEEE. <https://doi.org/10.1109/IGARSS46834.2022.9884716>
- Hopkinson, C., Fuoco, B., Grant, T., Bayley, S. E., Brisco, B., & MacDonald, R. (2020). Wetland hydroperiod change along the Upper Columbia River floodplain, Canada, 1984 to 2019. *Remote Sensing*, 12(24), 4084. <https://doi.org/10.3390/rs12244084>
- Hosseiny, B., Mahdianpari, M., Brisco, B., Mohammadimanesh, F., & Salehi, B. (2022). WetNet: A spatial-temporal ensemble deep learning model for wetland classification using Sentinel-1 and Sentinel-2. *IEEE Transactions on Geoscience and Remote Sensing*, 60, 1–14. <https://doi.org/10.1109/TGRS.2021.3113856>
- Kharazmi, R., Tavili, A., Rahdari, M. R., Chaban, L., Panidi, E., & Rodrigo-Comino, J. (2018). Monitoring and assessment of seasonal land cover changes using remote sensing: A 30-year (1987–2016) case study of Hamoun Wetland. *Iran. Environmental Monitoring and Assessment*, 190(6), 356. <https://doi.org/10.1007/s10661-018-6726-z>
- Kouhgardi, E., Hemati, M., Shakerdargah, E., Shiri, H., & Mahdianpari, M. (2022). Monitoring shoreline and land use/land cover changes in sandbanks provincial park using remote sensing and climate data. *Water*, 14(22), 3593. <https://doi.org/10.3390/w14223593>
- Li, J., & Chen, W. (2005). A rule-based method for mapping Canada's wetlands using optical, radar and DEM data. *International Journal of Remote Sensing*, 26(22), 5051–5069. <https://doi.org/10.1080/01431160500166516>
- Mahdianpari, M., Brisco, B., Granger, J. E., Mohammadimanesh, F., Salehi, B., & Banks, S., et al. (2020a). The second generation Canadian wetland inventory map at 10 meters resolution using Google Earth Engine. *Canadian Journal of Remote Sensing*, 46(3), 360–375. <https://doi.org/10.1080/07038992.2020.1802584>

- Mahdianpari, M., Brisco, B., Granger, J., Mohammadimanesh, F., Salehi, B., Homayouni, S., & Bourgeau-Chavez, L. (2021). The third generation of Pan-Canadian wetland map at 10 m resolution using multisource earth observation data on cloud computing platform. *IEEE Journal of Selected Topics in Applied Earth Observations and Remote Sensing*, *14*, 8789–8803. <https://doi.org/10.1109/JSTARS.2021.3105645>
- Mahdianpari, M., Salehi, B., Mohammadimanesh, F., Brisco, B., Homayouni, S., & Gill, E., et al. (2020b). Big data for a big country: The first generation of Canadian wetland inventory map at a spatial resolution of 10-m using Sentinel-1 and Sentinel-2 data on the Google Earth Engine cloud computing platform. *Canadian Journal of Remote Sensing*, *46*(1), 15–33. <https://doi.org/10.1080/07038992.2019.1711366>
- Mahdianpari, M., Salehi, B., Mohammadimanesh, F., Homayouni, S., & Gill, E. (2019). The first wetland inventory map of Newfoundland at a spatial resolution of 10 m using Sentinel-1 and Sentinel-2 data on the Google Earth Engine cloud computing platform. *Remote Sensing*, *11*(1), 43. <https://doi.org/10.3390/rs11010043>
- Mahdianpari, M., Salehi, B., Mohammadimanesh, F., & Motagh, M. (2017). Random forest wetland classification using ALOS-2 L-band, RADARSAT-2 C-band, and TerraSAR-X imagery. *ISPRS Journal of Photogrammetry and Remote Sensing*, *130*, 13–31. <https://doi.org/10.1016/j.isprsjprs.2017.05.010>
- Mao, D., Wang, Z., Du, B., Li, L., Tian, Y., & Jia, M., et al. (2020). National wetland mapping in China: A new product resulting from object-based and hierarchical classification of Landsat 8 OLI images. *ISPRS Journal of Photogrammetry and Remote Sensing*, *164*, 11–25. <https://doi.org/10.1016/j.isprsjprs.2020.03.020>
- Millennium Ecosystem Assessment. (2005). Retrieved May 2, 2021, from <https://www.millenniumassessment.org/en/index.html>
- Minaei, M., & Kainz, W. (2016). Watershed land cover/land use mapping using remote sensing and data mining in Gorganrood. *Iran. ISPRS International Journal of Geo-Information*, *5*(5), 57. <https://doi.org/10.3390/ijgi5050057>
- Mitsch, W. J., Bernal, B., Nahlik, A. M., Mander, Ü., Zhang, L., & Anderson, C. J., et al. (2013). Wetlands, carbon, and climate change. *Landscape Ecology*, *28*(4), 583–597. <https://doi.org/10.1007/s10980-012-9758-8>
- Munyati, C. (2000). Wetland change detection on the Kafue Flats, Zambia, by classification of a multitemporal remote sensing image dataset. *International Journal of Remote Sensing*, *21*(9), 1787–1806. <https://doi.org/10.1080/014311600209742>
- Ozesmi, S. L., & Bauer, M. E. (2002). Satellite remote sensing of wetlands. *Wetlands Ecology and Management*, *10*(5), 381–402. <https://doi.org/10.1023/A:1020908432489>
- Qaderi Nasab, F., & Rahnama, M. B. (2020). Developing restoration strategies in Jazmurian wetland by remote sensing. *International Journal of Environmental Science and Technology*, *17*(5), 2767–2782. <https://doi.org/10.1007/s13762-019-02568-0>
- Qureshi, S., Alavipannah, S. K., Konyushkova, M., Mijani, N., Fathololomi, S., & Firozjaei, M. K., et al. (2020). A remotely sensed assessment of surface ecological change over the Gomishan Wetland. *Iran. Remote Sensing*, *12*(18), 2989. <https://doi.org/10.3390/rs12182989>
- Ramsar Convention. (2016). Ramsar handbook 5th edition.
- Ramsar Convention Secretariat. (2013). The Ramsar convention manual, 6th edition. Retrieved January 18, 2021, from <https://www.ramsar.org/document/the-ramsar-convention-manual-6th-edition>
- Rezaee, M., Mahdianpari, M., Zhang, Y., & Salehi, B. (2018). Deep convolutional neural network for complex wetland classification using optical remote sensing imagery. *IEEE Journal of Selected Topics in Applied Earth Observations and Remote Sensing*, *11*(9), 3030–3039. <https://doi.org/10.1109/JSTARS.2018.2846178>
- Rodriguez-Galiano, V. F., Ghimire, B., Rogan, J., Chica-Olmo, M., & Rigol-Sanchez, J. P. (2012). An assessment of the effectiveness of a random forest classifier for land-cover classification. *ISPRS Journal of Photogrammetry and Remote Sensing*, *67*, 93–104. <https://doi.org/10.1016/j.isprsjprs.2011.11.002>
- Rundquist, D. C., Narumalani, S., & Narayanan, R. M. (2001). A review of wetlands remote sensing and defining new considerations. *Remote Sensing Reviews*, *20*(3), 207–226. <https://doi.org/10.1080/02757250109532435>
- Salehi, B., Mahdianpari, M., Amani, M., Manesh, F., Granger, J., Mahdavi, S., & Brisco, B. (2019). A collection of novel algorithms for wetland classification with SAR and optical data. In D. Gökçe (Ed.), *Wetlands Management - Assessing Risk and Sustainable Solutions*. IntechOpen. <https://doi.org/10.5772/intechopen.80688>
- Salehi, B., Zhang, Y., Zhong, M., & Dey, V. (2012). Object-based classification of urban areas using VHR imagery and height points ancillary data. *Remote Sensing*, *4*(8), 2256–2276. <https://doi.org/10.3390/rs4082256>
- Schmitt, A., & Brisco, B. (2013). Wetland monitoring using the curvelet-based change detection method on polarimetric SAR imagery. *Water*, *5*(3), 1036–1051. <https://doi.org/10.3390/w5031036>
- Scott, D. A., & Jones, T. A. (1995). Classification and inventory of wetlands: A global overview. *Vegetatio*, *118*(1–2), 3–16. <https://doi.org/10.1007/BF00045186>
- Sheykhmousa, M., Mahdianpari, M., Ghanbari, H., Mohammadimanesh, F., Ghamisi, P., & Homayouni, S. (2020). Support vector machine versus random forest for remote sensing image classification: A meta-analysis and systematic review. *IEEE Journal of Selected Topics in Applied Earth Observations and Remote Sensing*, *13*, 6308–6325. <https://doi.org/10.1109/JSTARS.2020.3026724>
- Song, X. -P., Hansen, M. C., Stehman, S. V., Potapov, P. V., Tyukavina, A., Vermote, E. F., & Townshend, J. R. (2018). Global land change from 1982 to 2016. *Nature*, *560*(7720), 639–643. <https://doi.org/10.1038/s41586-018-0411-9>
- Tiner, R. W., Lang, M. W., & Klemas, V. (Eds.). (2015). *Remote sensing of wetlands: applications and advances*. Boca Raton: CRC Press, Taylor & Francis Group.
- UN. (2019). World Population Prospects - Population Division - United Nations. Retrieved August 11, 2020, from <https://population.un.org/wpp/>
- Venter, Z. S., & Sydenham, M. A. K. (2021). Continental-scale land cover mapping at 10 m resolution over Europe (ELC10). *Remote Sensing*, *13*(12), 2301. <https://doi.org/10.3390/rs13122301>
- Walker, W. S., Stickler, C. M., Kelldorfer, J. M., Kirsch, K. M., & Nepstad, D. C. (2010). Large-area classification and mapping of forest and land cover in the Brazilian

- Amazon: A comparative analysis of ALOS/PALSAR and Landsat data sources. *IEEE Journal of Selected Topics in Applied Earth Observations and Remote Sensing*, 3(4), 594–604. <https://doi.org/10.1109/JSTARS.2010.2076398>
- Wdowinski, S., Kim, S. -W., Amelung, F., Dixon, T. H., Miralles-Wilhelm, F., & Sonenshein, R. (2008). Space-based detection of wetlands' surface water level changes from L-band SAR interferometry. *Remote Sensing of Environment*, 112(3), 681–696. <https://doi.org/10.1016/j.rse.2007.06.008>
- Whiteside, T. G., & Bartolo, R. E. (2015). Mapping aquatic vegetation in a tropical wetland using high spatial resolution multispectral satellite imagery. *Remote Sensing*, 7(9), 11664–11694. <https://doi.org/10.3390/rs70911664>
- Wulder, M., Li, Z., Campbell, E., White, J., Hobart, G., Hermosilla, T., & Coops, N. (2018). A national assessment of wetland status and trends for Canada's forested ecosystems using 33 years of earth observation satellite data. *Remote Sensing*, 10(10), 1623. <https://doi.org/10.3390/rs10101623>
- Yousefi, M., Kafash, A., Valizadegan, N., Ilanloo, S. S., Rajabizadeh, M., & Malekoutikhah, S., et al. (2019). Climate change is a major problem for biodiversity conservation: A systematic review of recent studies in Iran. *Contemporary Problems of Ecology*, 12(4), 394–403. <https://doi.org/10.1134/S1995425519040127>

Publisher's Note Springer Nature remains neutral with regard to jurisdictional claims in published maps and institutional affiliations.

Springer Nature or its licensor (e.g. a society or other partner) holds exclusive rights to this article under a publishing agreement with the author(s) or other rightsholder(s); author self-archiving of the accepted manuscript version of this article is solely governed by the terms of such publishing agreement and applicable law.